A Platinum Open Access Journal for Organic Chemistry

Paper

Free to Authors and Readers | DOAJ Seal | *Arkivoc* **2026** (3) 202612595

Photophysical and antibacterial properties of symmetrical curcuminoid–BF_2 complexes

David J. Vass,[a] Balázs Brém,[a] Carmen R. Pop,[b] Castelia Cristea,[a] Emese Gál,*[a] and Luiza Gaina*[a]

[a]Faculty of Chemistry and Chemical Engineering, Babeș-Bolyai University, Arany János No. 11, 400028 Cluj-Napoca, Romania; [b] Department of Food Science, Faculty of Food Science and Technology, University of Agricultural Sciences and Veterinary Medicine of Cluj-Napoca, Calea Florești No. 64, 400509 Cluj-Napoca, Romania

Email: emese.gal@ubbcluj.ro, ioana.gaina@ubbcluj.ro

This article is dedicated to Prof. Thomas J. J. Müller for his outstanding contribution to Organic Chemistry

Received 04-09-2026 **Accepted** 05-08-2026 **Published on line** 05-17-2026

Abstract

Difluoroboron complexes of curcumin derivatives carrying methoxy- or chloro-substituents in various positions of the aromatic rings were synthesized, and their photophysical and antibacterial properties were evaluated. The position of their UV-Vis absorption/emission maxima was found to highly depend on the substituents' electronic effect and solute-solvent interactions. The 4-methoxy-substituted analogue showed the largest bathochromic shift of the UV-Vis absorption maxima and Stokes shift of the fluorescence emission maxima. Time Dependent Density Functional Theory (TD-DFT) employed in the modelling of the optical properties of these organic dyes provided reasonably accurate results in both gas phase and solvated systems. Their antibacterial effect against Gram-negative and Gram-positive bacteria appeared strongly influenced by their dipole moment and sensitivity to nucleophiles. The 4-chloro-substituted analogue gave the best inhibition against *S. enteritidis* and *S. aureus*, while the 3-methoxy-substituted analogue exhibited the strongest response against *E. coli* and *L. monocytogenes* strains.

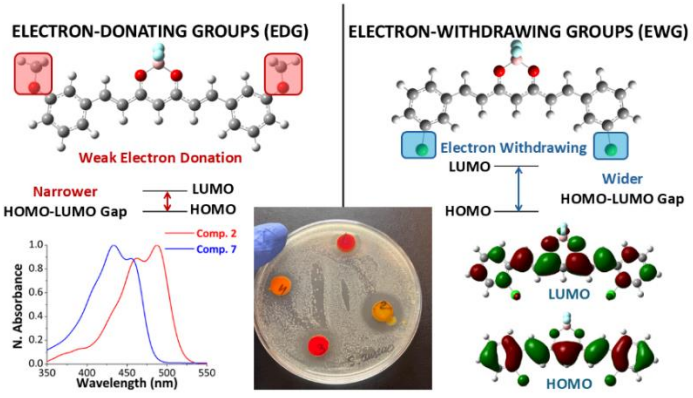

Keywords: Symmetrical curcuminoid; optical properties; antibacterial activities; TD-DFT

Cite as *Arkivoc* 2026 (3) 202612595
DOI: https://doi.org/10.24820/ark.5550190.p012.595

Introduction

Curcumin *(1E,6E)*-1,7-*bis*(4-hydroxy-3-methoxyphenyl)-hepta-1,6-diene-3,5-dione is the primary polyphenolic diarylheptanoid isolated from *Curcuma longa*. This unsaturated β-diketone exists in a dynamic tautomeric equilibrium; however, the enolic form predominates, characterized by a planar geometry and a highly delocalized π electron system extending across the molecular backbone. This extensive conjugation is fundamental to its unique photophysical profile, facilitating long wavelength absorption and stabilizing radical species, which underpins its diverse biological and chemical utility.[1]

Extensive clinical research over the past three decades has scrutinized the therapeutic potential of curcumin. These investigations have established a robust pharmacological profile, demonstrating that curcumin and its synthetic analogues possess potent antioxidant, anti-inflammatory, antibacterial, and antiviral properties.[2] As a result of the low C–H bond dissociation enthalpy in the *meso* positioned methylene group, and due to its phenolic hydroxyl groups, curcumin can easily degrade in the presence of free radicals, Reactive Oxygen Species (ROS), and UV light.[3–5] The susceptibility of the diketo form toward nucleophiles renders curcumin unstable under basic conditions. This vulnerability leads to the cleavage of the heptadienone chain, resulting in the formation of ferulic acid and feruloylmethane.[6]

In its enolic form, curcumin can act as a bidentate ligand. Upon deprotonation, it coordinates to metal centres through the oxygen atoms of the enol and carbonyl groups, forming a stable six membered chelate ring with a delocalized π electron system. Upon complexation, the lipophilicity of curcuminoids increases, the cellular uptake, bioavailability and bioactivity improve, and thus the antioxidant, anti-inflammatory, antimicrobial, and antiviral effects are stronger compared to the free ligands.[7] Numerous metal curcuminoid complexes have been successfully isolated and characterized, highlighting the versatility of the curcumin scaffold in coordination chemistry.[8] Among the most extensively investigated derivatives are the difluoroboron curcuminoids (BF_2 complexes), which have garnered significant attention due to their unique electronic properties. These are more stable due to chelate formation, which is thermodynamically favoured and possesses internal resonance. This internal resonance facilitates the π electron conjugated system extended on the entire chromophore and increases the ligand's structural rigidity, leading to a bathochromic shift in the UV-Vis spectra.[9-11]

A significant challenge in the field remains the efficient synthesis of curcumin analogues via amine catalysed aldol condensation between acetylacetone and aromatic aldehydes, specifically focusing on methodologies that preclude the need for labour intensive purification steps. There are two major pathways frequently described in the literature with the main difference consisting in the procedure applied for the protection of the *meso* positioned methylene group of acetylacetone against alkylation during aldol condensation: one method using boron oxide (described by Pabon *et al.*[12]), and the another recommending boron trifluoride etherate (described by Rao[13]) in the protection step. In the acetylacetone boron oxide complex, the boron centre is highly electrophilic; consequently, this intermediate is exceedingly sensitive to moisture and other weak nucleophiles.[12] On the other hand, the thermodynamically favoured BF_2 chelate is further stabilized by internal resonance, and thus it possesses high stability.[13]

In this context, the present work aims to report the straightforward synthesis, structural and photophysical characterization, and antibacterial evaluation of a systematic series of symmetrical difluoroboron curcuminoid complexes. These complexes feature a 1,7-bis(phenyl)hepta-1,6-diene-3,5-dione chromophore, functionalized with methoxy or chloro auxochromes at the *ortho*, *meta*, or *para* positions of the peripheral aromatic rings. Furthermore, their properties were corroborated by computational investigations using density functional theory (DFT) and time dependent DFT (TDDFT).

Results and Discussion

Synthetic procedures

The synthetic pathway applied in the preparation of the target difluoroboron complexes of curcumin derivatives **2-8** is presented in Scheme 1. In this two steps procedure intermediate acetylacetone difluoroboronite **1** was prepared primarily by the reaction of acetylacetone with boron trifluoride etherate, followed by the condensation of **1** with a series of substituted benzaldehydes (2-, 3-, 4-methoxybenzaldehyde and 2-, 3-, 4-chlorobenzaldehyde respectively).

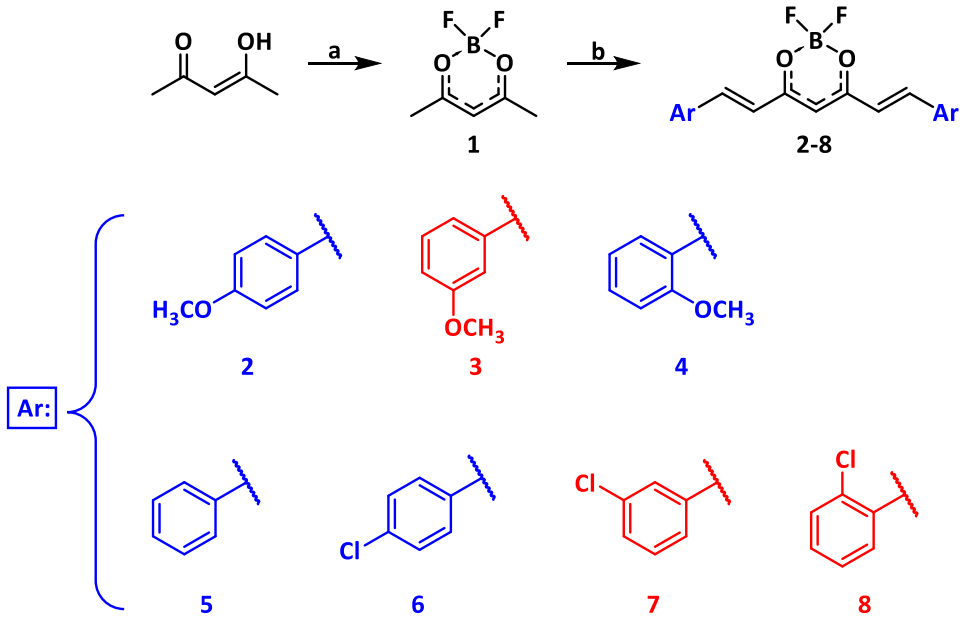

Scheme 1. Synthesis of symmetrical curcuminoid BF_2-complexes (the novel compounds marked with red)
a: BF_3·THF, DCM, r.t., 16 h; **b:** aromatic aldehyde, $B(OBu)_3$, $BuNH_2$, EtOAc, r.t.

Acetylacetone difluoroboronite **1** was first synthesized by Gilbert *et al.* in 1924 via bubbling BF_3 gas into acetylacetone.[14] The first modification of the experiment was done by Crimmins *et al.* in 1967 by using acetic anhydride as solvent, gaining a yield around 20 %.[15] Two years later, Brown *et al.* recommended using boron-trifluoride etherate instead of boron trifluoride gas for easier handling and a lipophilic solvent in which each starting material is miscible, obtaining a yield around 55 %.[16] In the present research, the synthesis of compound **1** was carried out in both anhydrous dichloromethane (DCM) and in anhydrous toluene solvents respectively. The reaction yield achieved in DCM was around 74% while in toluene it was obtained only 21%. Since both starting materials are miscible with toluene, the interaction between the aromatic solvent's delocalized π-electron system and boron trifluoride probably blocked the ligand substitution on the boron centre.

Compounds **2**,[17] **4**,[18] **5** and **6**[19] have already been synthesized and described in the literature. Yields range from approximately 35% to 45% for the Pabon method,[11] (which involves the synthesis of acetylacetone-boron acid complex, an amine catalysed aldol condensation, resulting the boron oxy complex of the corresponding curcumin analogue) and from 70% to 95% for the Rao method (complexation of acetylacetone and BF_3·Et_2O, followed by condensation with the corresponding benzaldehyde analogues).[13] The results obtained by the procedure applied in this work match the previous literature reports, affording better conversions in the

reaction with benzaldehyde derivatives containing strong electron donating groups (*HRMS spectra in ESI Figure 1.1-1.7*). The condensation of **1** with nitro benzaldehydes failed despite the nature of the solvent employed.

Structural characterization

Molecular modelling based on density functional theory (DFT) was applied to determine the molecular geometry at gas phase ground state *(see Cartesian coordinates in ESI)*. In the dioxaborine ring, the boron atom is sp^3 hybridized, hence it has a distorted tetrahedral geometry. This lowers the symmetry of the molecules, therefore all difluoroboron curcuminoid complexes belong to C_1 point group. The CO bonds are equivalent, with a bond length of 1.30 Å, which is around 7 pm longer than the usual C=O bonds, and 10 pm shorter than the usual enolic C–O bonds.[20] In the experimentally recorded ^{13}C NMR spectrum, the two carbon atoms in the CO groups are equivalent, displaying isochronous signals situated around 190 ppm. These results support the electron delocalization in the boron oxy chelate. In the unsaturated aliphatic chain, the single C-C bonds are 9 pm shorter, and the C=C bonds are 2 pm longer than in the corresponding carbon carbon bonds typical of alkanes and alkenes.[20] This is a consequence of the π electron conjugated system extended on the entire molecular backbone. These results correlate with the DFT data already published by Canard *et al.*[18] In the ^{1}H NMR spectra of **2-8**, the vinyl protons displayed split signals with coupling constants of approximately 15.5 Hz, pointing towards a diastereoselectivity for *all trans* isomer at room temperature.

In the ^{1}H NMR spectra of **2-8**, the chemical shifts displayed by the protons attached to the *meso* positioned methine groups are clear indicators of the electron donating properties of the substituents pending to the aryl units. Therefore, the recorded chemical shift for the reference compound **5** (containing unsubstituted phenyl rings) was 6.15 ppm, while for the other complexes, the corresponding chemical shifts values appeared to be smaller due to the shielding effect exerted by the electron donating substituents. The π electron donating effect of the methoxy group was observable for each of *ortho* and *para* position isomers, but in *meta* position the effect appeared almost negligible. The chlorine substituent exhibited electron donating effect only when attached in the *para* position of the aromatic rings; *ortho* and *meta* chloro substituted auxochromes showed predominantly an electron withdrawing effect. *(ESI Figure 2.1-2.40)* In the ^{11}B and ^{19}F NMR spectra, the chemical shifts are not notably influenced by substituent electronic effects, unlike those in ^{1}H and ^{13}C NMR. The ^{11}B NMR chemical shifts ranged from 1.06 to 1.94 ppm, and in the ^{19}F NMR the chemical shifts ranged from -136.93 to -140.33 ppm. The most deshielded values in both measurements were observed for compound 7, where the meta chlorine substituent led to the greatest decrease in electron density on the boron and fluorine nuclei.

Photophysical properties

The optical properties of the difluoroboron curcuminoids **2-8** investigated by UV-Vis absorption/emission spectroscopy are summarized in Table 1 (*also ESI Table S1 and Table S2*). Difluoroboron curcuminoid derivative **5** (containing unsubstituted phenyl rings), representing the base chromophore system, exhibited absorption maxima ranging from 450 to 460 nm in solvents of different polarities (which correlates with values already published in the literature.[21] TDDFT calculations specify that this corresponds to a HOMO-LUMO electronic transition.[19] A close inspection of the data in Table 1 indicates a bathochromic shift of the absorption maxima induced by the *methoxy* auxochrome, and a hypsochromic shift brought by the chlorine auxochrome. The highest absorption maxima were displayed by the *para* methoxy substituted derivative **2** (480 – 500 nm), followed by its *ortho* analogue **4**, in agreement with previously reported values.[19] The novel *ortho* and *meta* chloro substituted difluoroboron curcuminoids **7** and **8** displayed a hypsochromic shift of the absorption maxima in comparison with the *para* isomer **6**.

The DFT computational results are presented in Figure 1, showing the shape and energies of the frontier molecular orbitals (FMO) involved in the electronic transitions of **7** and **8**. The results reveal a larger energy gap for the *ortho* chloro substituted isomer **8,** in good agreement with the experimental UV-Vis absorption spectra**.** The HOMO–LUMO energy gap was theoretically estimated under vacuum conditions as well as in the presence of solvents of different polarity. Figure 1 illustrates the spatial distribution and energies of the frontier molecular orbitals (HOMO and LUMO) for the newly synthesized compounds **7** and **8**.

Table 1. UV-Vis absorption and fluorescence emission data of difluoroboron curcuminoids **2**-**8** experimental versus computational data

No.	Solvent	λ_{abs} Exp. (nm)	λ_{abs} Calc. (nm)	λ_{em} Exp. (nm)	λ_{em} Calc. (nm)	Stokes shifts Exp. (cm^{-1})
	Gas	–	443	–	464	–
	Toluene	488	485	527	515	1516
2	DCM	489	497	541	564	1966
	DMSO	498	503	553	585	1997
	MeOH	482	498	550	583	2565
	Gas	–	443	–	506	–
	Toluene	457	476	499	510	1842
3	DCM	455	485	506	549	2097
	DMSO	463	489	508	566	1913
	MeOH	450	486	493	564	1938
	Gas	–	430	–	456	–
	Toluene	474	468	520	502	1866
4	DCM	474	482	526	547	2158
	DMSO	486	488	550	566	2394
	MeOH	469	483	534	564	2595
	Gas	–	414	–	443	–
	Toluene	449	447	465	485	1947
5	DCM	449	454	475	525	2740
	DMSO	458	457	491	542	1216
	MeOH	443	453	476	540	1565
	Gas	–	427	–	456	–
	Toluene	456	459	500	499	698
6	DCM	456	465	484	538	1396
	DMSO	462	468	491	555	1278
	MeOH	449	464	485	553	1653

Table 1. Continue

No.	Solvent	λabs Exp. (nm)	λabs Calc. (nm)	λem Exp. (nm)	λem Calc. (nm)	Stokes shifts Exp. (cm^{-1})
7	Gas	–	414	–	455	–
	Toluene	447	444	465	484	866
	DCM	446	449	470	521	1008
	DMSO	453	452	473	537	933
	MeOH	440	448	467	535	1314
8	Gas	–	412	–	445	–
	Toluene	429	442	481	484	1432
	DCM	427	448	476	520	1401
	DMSO	434	451	492	535	1653
	MeOH	420	447	479	553	721

The graphical representation shows that the electron density is predominantly localised on the phenyl ring, which constitutes the major contribution to the HOMO. In contrast, vertical excitation leads to population of the LUMO, where the electron density is more concentrated on the difluoroboron acetylacetonate fragment.

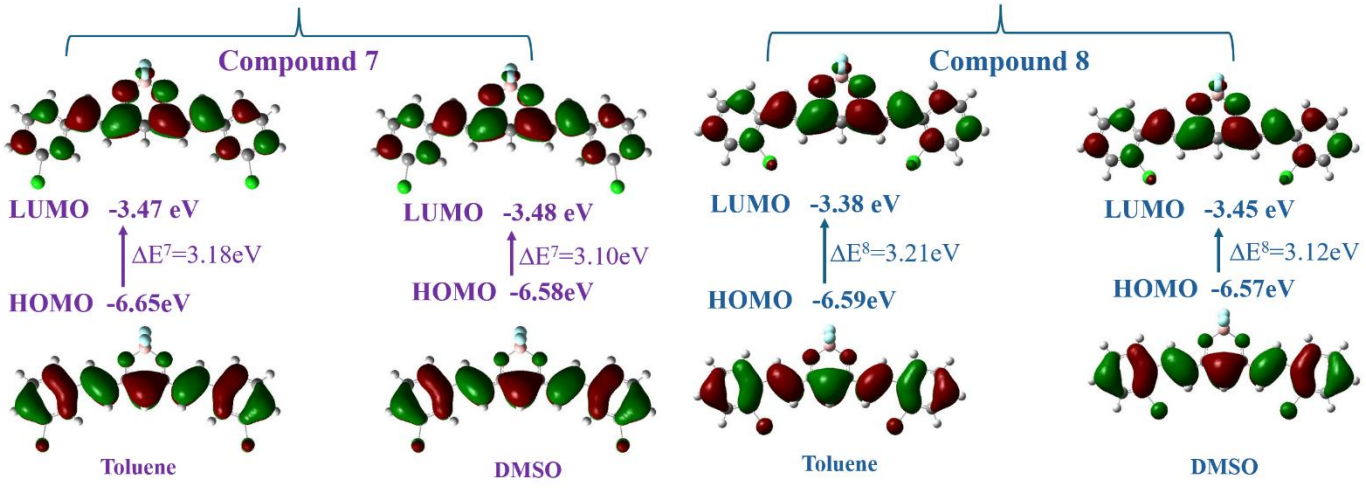

Figure 1. Frontier Molecular Orbitals for compounds **7** and **8** in solvents with various polarities.

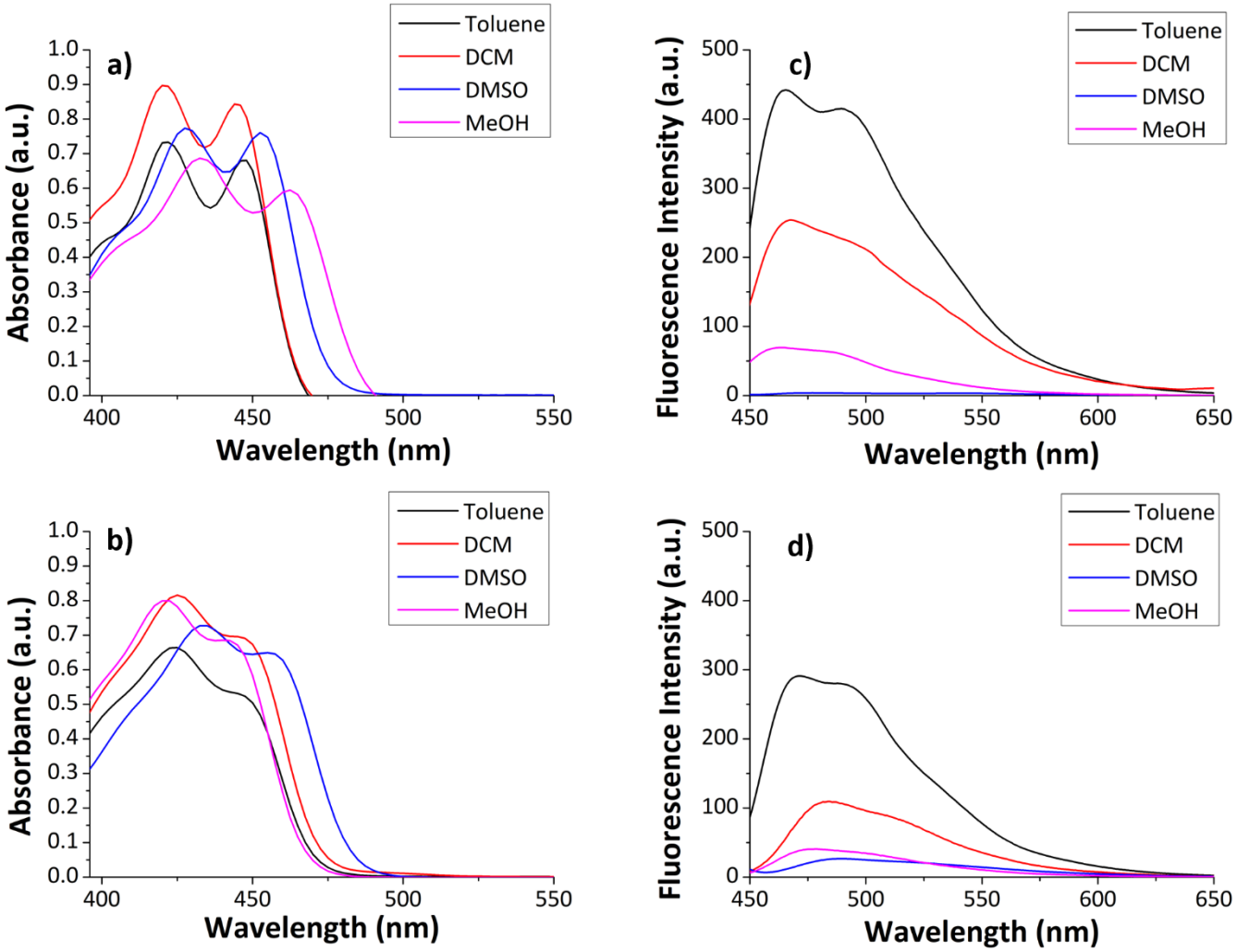

Figure 2. a) The absorbance spectra of **7** in several solvents (16 µM, r.t.); b) The absorbance spectra of **8** in several solvents (15 µM, r.t.); c) The emission spectra of **7** in several solvents (1.07 µM, r.t.); c) The emission spectra of **8** in several solvents (5.50 µM, r.t.).

Examination of electronic transitions in the UV-Vis region specifies strong correlation between solute solvent interactions and absorption/emission spectra (*ESI Figure 3.1-3.10*). Compounds **2-8** are highly polar and thus proficient in developing dipole dipole solute solvent interactions with polar solvents such as DMSO, methanol and DCM. The TDDFT computational results suggest that the solvent solute interactions slightly increase the HOMO energy and strongly decrease the LUMO energy diminishing the energy requirement for the vertical electron excitation and producing a red shift of the absorption maximum (*ESI Table S4*). Similar trends were observed by Ekici & Karakus¸ on 4-aminouracil derivatives.[22]

As can be concluded from Figure 2, compounds **7** and **8** possess strong emission in weakly polar solvents, however the fluorescence intensities in hydrogen acceptor polar solvents are noteworthily smaller. Via the lone electron pairs from the electron rich oxygen atoms, these solvent molecules can interact with the unoccupied orbitals from the boron atom, forming stable adducts, which upon singlet excitation, relax to ground state through solvent relaxation instead of photon emission. Upon excitation with the characteristic absorption maxima, each difluoroboron curcuminoid **2-8** displayed fluorescence emissions with large Stokes shifts

summarized in Table 1. The previously reported compounds show fluorescence emissions having fluorescence relative quantum yield in solution around ϕFl = 0.29 for **5** in toluene,[22] 0.44 for **2** and 0.32 for **4** in DCM.[18]

Table 2. Fluorescence quantum yields for the synthesized compounds

Compound	*ϕFl in solution**	*ϕFl in solid*
2	0.29 c = 0.07 µM	0.08
3	0.37 c = 0.47 µM	0.06
4	0.24 c = 0.25 µM	0.14
6	0.12 c = 0.57 µM	0.12
7	0.13 c = 1.06 µM	0.03
8	0.10 c = 5.50 µM	0.01

** in toluene solvent*

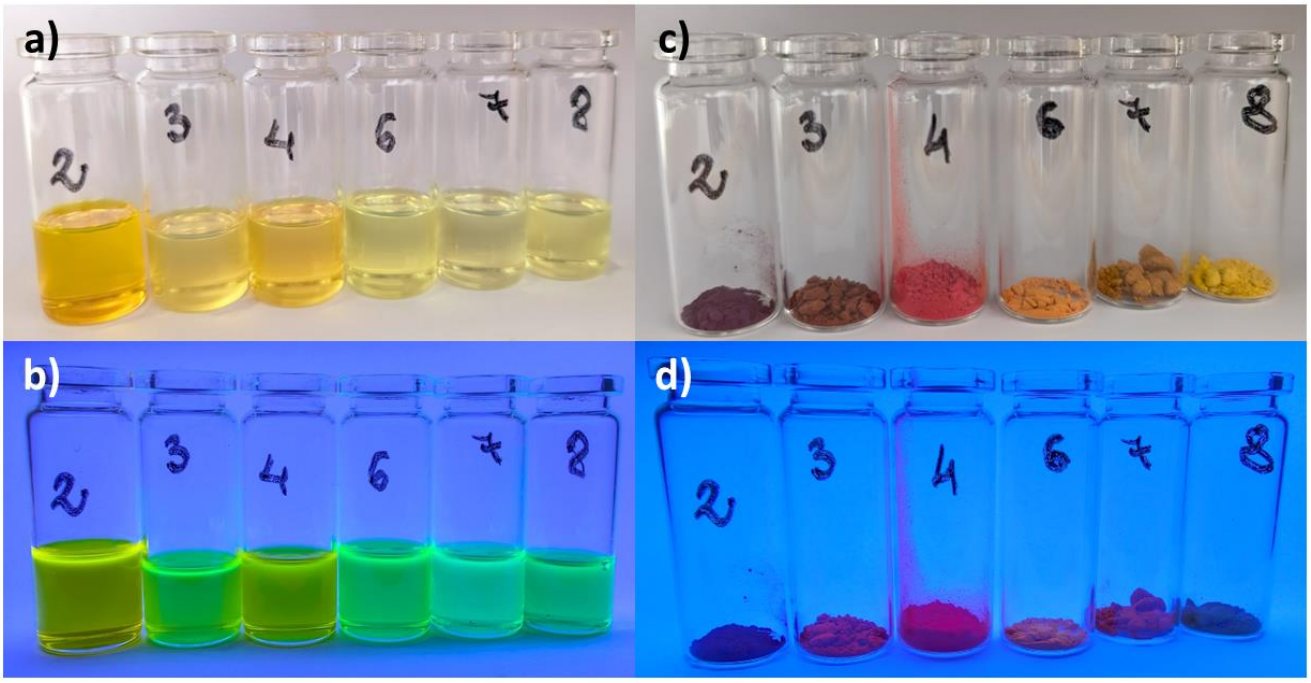

Figure 3. Solution of the synthesized compounds in toluene **a)** in natural light **b)** under a 395 nm UV lamp. The solids **c)** in natural light and **d)** under a 395 nm UV lamp.

According to the experimental data summarized in Table 2 (and as can be seen on Figure 3), curcumin difluoroboron complexes with strong electron donating moieties possess better absolute fluorescence quantum yields overall both in toluene solution and in solid state. For the newly synthesized compounds **3**, **7** and **8** the

absolute fluorescence quantum yield was ϕFl = 0.29, 0.13 and 0.10 in solution, and ϕFl = 0.06, 0.03 and 0.01 in powder. The largest Stokes shifts occurred in DMSO (2390 – 7360 cm^{-1}), followed by DCM (2540 – 2820 cm^{-1}), then methanol (2620 – 3250 cm^{-1}) and lastly in toluene solvent (2020 – 2840 cm^{-1}). For instance, upon photoexcitation, compound **2** exhibits an increase in dipole moment of approximately 1.5 D (*ESI Table S3*), indicating a more polar excited state. Consequently, highly polar solvents can stabilize the excited state species to a greater extent than the nonpolar ones with an aromatic backbone. This enhanced excited state solvation leads to increased solvent reorganization and, therefore, greater energy dissipation in polar solvents relative to less polar or nonpolar ones. Comparable trends in excited-state polarity and solvent-dependent stabilization have been previously reported by Ghosh et al. for parent curcumin.[23]

Antimicrobial activity

The antibacterial activity of the curcuminoid BF_2 complexes **2-8** was investigated on different Gram-negative (*Escherichia coli*, *Salmonella enteritidis*) and Gram positive bacteria (*Staphylococcus aureus, Listeria monocytogenes*) and compared with Gentamicin standard (Table 3). According to the data already published, compound **2** does not have toxicity against *Fusarium oxysporum* fungi at 100 µM concentration in dark media,[24] as well as compound **5** did not give any toxicity against *Aliivibrio fischeri* bacteria at 100 µM concentration.[25] As our results show, complexes possessing methoxy group have better antibacterial activity against the tested strains overall. From these, compound **3** gave a remarkable 21.7 mm inhibition diameter in the case of *L. monocytogenes*, which is only 2.5 mm smaller than the reference gentamicin's. According to the dipole moments gained *in silico*, compound **3** is the least polar from the synthesized methoxy analogues in DMSO, and containing weak electron donating substituents, it makes them more stable in physiological conditions. This leads to better absorption through the double layered phospholipid cell membrane, and the absorbed molecules persist longer inside the bacteria. Following the DFT results, from chlorine containing analogues, compounds **7** and **8** are the least polar in DMSO, having dipole moments 6 and 7 Debye respectively. In contrast, compound **6** gave the largest inhibition diameters overall against *S. enteritis* and *S. aureus*, and compound **7** did not show antibacterial effect at all. Compound **5** showed weak antimicrobial effect; thus, substituents are required for advanced bioactivity.

Table 3. The measured inhibition diameters of the synthesized compounds

Compound	Sample concentration	*Escherichia coli* ATCC 25922	*Salmonella enteritidis* ATCC 13076	*Staphylococcus aureus* ATCC 6538P	*Listeria monocytogenes* ATCC 19114
	µM	(mm)	(mm)	(mm)	(mm)
2	124	15.2 15.7	14.2 14.0	14.5 15.7	9.0 9.5
3	126	21.0 20.6	19.0 18.9	19.0 20.0	23.5 24.0
4	125	13.8 12.5	12.5 12.0	12.5 13.0	21.5 22.0

Table 3. Continue

Compound	Sample concentration	Escherichia coli ATCC 25922	Salmonella enteritidis ATCC 13076	Staphylococcus aureus ATCC 6538P	Listeria monocytogenes ATCC 19114
	µM	(mm)	(mm)	(mm)	(mm)
5	128	10.0 9.3	9.2 9.8	11.5 10.6	12.5 12.2
6	125	20.0 20.7	22.0 21.6	20.5 21.2	19.5
7	125	-	-	-	-
8	125	14.0 13.6	11.0 10.6	16.5 16.0	13.6 14.2
DMSO	-	-	-	-	-
Gentamicin	85	29.3 29.7	27.5 27.0	26.5 27.0	25.8 26.0

Conclusions

This study described the synthesis of a systematic series of symmetrical difluoroboron curcuminoid complexes containing a 1,7-*bis*(phenyl)-hepta-1,6-diene-3,5-dione chromophore system decorated with methoxy or chloro auxochromic substituents attached in the *ortho, meta* or *para* position of the peripheral aromatic rings and reported their photophysical and antibacterial properties *via* experimental and theoretical methods. It was shown that the electronic effect of the substituents highly influences the photophysical properties of the complexes. The electron donating substituents widen the electron density on the chromophore, increasing the FMOs' energy, leading to a strong bathochromic shift of the absorption maxima. Solvent solute interactions with polar solvents such as DMSO decrease the LUMOs' energy and cause a red shift of the absorption maxima. The stronger solute solvent interactions are, the stronger the solvent relaxation is, therefore the Stokes shift increases the most in DMSO. The antimicrobial properties of the difluoroboron curcuminoid complexes were found to depend on their polarity helping them pass through the cell membrane, as well as affecting their stability in the cells.

Experimental Section

General. The HRMS spectra were acquired on a Thermo LTQ Orbitrap XL mass spectrometer, utilising either atmospheric pressure chemical ionization (APCI+) in positive ion mode. The NMR spectra were recorded on a

Bruker Advance 400 MHz and 600 MHz spectrometers. All measurements were performed in $CDCl_3$, with chemical shifts (δ) reported in ppm relative to the residual solvent signal δ 7.26 for ^1H and δ 77.16 for ^{13}C NMR.

Synthesis of acetylacetone BF_2 complex (1). A 250 mL Schlenk tube was charged with 50 mL of anhydrous DCM, then 1 eq. (101 mmol, 10.1 g, 10.3 mL) acetylacetone and 1,5 eq. (152 mmol, 70.9 g, 55.2 mL) 30% BF_3·THF solution were added. The reaction mixture was stirred overnight at room temperature under an argon atmosphere. Upon completion, the solvents were distilled off, and the reaction crude was kept in a refrigerator for one day. The formed solid was mixed with *n*-pentane, separated via vacuum filtration, and dried in vacuo (r.t, 15 mbar, 3h) to afford compound **1** as pale yellow needle crystals. Yield: 74% (11.1 g, 75 mmol).

General synthetic procedure of curcuminoid BF_2 complexes (2-8). A 250 mL oven dried Schlenk flask was charged with 2 eq. (28 mmol) aromatic aldehyde and 1 eq. (14 mmol, 2.1 g) compound **1,** and they were dissolved in 25 mL anhydrous ethylacetate under an argon atmosphere. After stirring at room temperature for 30 min, 5 mL tributylborate was added. After another 30 min stirring in the corresponding conditions, 1 eq. (14 mmol, 1.0 g, 1.4 mL) butylamine was added dropwise, and the reaction mixture was stirred overnight at room temperature. The reaction completion was monitored via TLC, using a 1:1 mixture of ethyl acetate and petroleum ether as eluent. Upon completion, the reaction was quenched via adding 10 mL of 1 M HCl solution. The forming precipitate was filtered off, washed thoroughly with distilled water, then dried in vacuo.

(1E,6E)-5-(Difluoroboryloxy)-1,7-bis(4-methoxyphenyl)-1,6-heptadiene-3,5-dione (2). Purple solid. Yield: 91% (4.9 g, 12.7 mmol). ^1H NMR (400 MHz, $CDCl_3$) δ (ppm): 8.01 (d, $^3J_{H3\text{-}H4}$ 15.5 Hz, 2H, H_3), 7.59 (d, $^3J_{H6\text{-}H7}$ 8.7 Hz, 4H, H_6), 6.96 (d, $^3J_{H6\text{-}H7}$ 8.7 Hz, 4H, H_7), 6.60 (d, $^3J_{H3\text{-}H4}$ 15.5 Hz, 2H, H_4), 6.03 (s, 1H, H_1), 3.90 (s, 6H, H_9). ^{13}C NMR (101 MHz, $CDCl_3$) δ (ppm): 179.5 (2C, C_2), 162.8 (2C, C_8), 146.9 (2C, C_3), 131.2 (4C, C_6), 127.0 (2C, C_5), 118.1 (2C, C_4), 114.8 (4C, C_7), 101.7 (1C, C_1), 55.5 (2C, OCH_3). ^{11}B NMR (128 MHz, $CDCl_3$) δ: 1,03 ppm. ^{19}F NMR (376 MHz, $CDCl_3$) δ: -140.33 ppm. APCI(+) HRMS calculated for $C_{21}H_{19}BF_2O_4$ [M-F]: 365.1360, found: 365.1359.

(1E,6E)-5-(Difluoroboryloxy)-1,7-bis-(3-methoxyphenyl)-1,6-heptadiene-3,5-dione (3). Bright purple solid. Yield: 83% (4.5 g, 11.6 mmol). ^1H NMR (400 MHz, $CDCl_3$) δ (ppm): 8.03 (d, $^3J_{H3\text{-}H4}$ 15.6 Hz, 2H, H_3), 7.37 (t, $J_{H7\text{-}H8\text{-}H9}$ 8.0 Hz, 2H, H_7), 7.23 (d, $^3J_{H6\text{-}H7}$ 7.8 Hz, 2H, H_6), 7.19 (t, *J* 2,1 Hz, 2H, H_{10}), 7.04 (dd, $^3J_{H7\text{-}H8}$ 8,2 Hz, ^4J 1,8 Hz 2H, H_8), 6.74 (d, $^3J_{H3\text{-}H4}$ 15.6 Hz, 2H, H_4), 6.15 (s, 1H, H_1), 3.88 (s, 6H, H_{11}). ^{13}C NMR (150 MHz, $CDCl_3$) δ (ppm): 180.3 (2C, C_2), 160.1 (2C, C_9), 147.6 (2C, C_3), 135.3 (2C, C_5), 130.2 (2C, C_7), 121.9 (2C, C_6), 120.8 (2C, C_4), 117.9 (2C, C_8), 113.9 (2C, C_{10}), 102.3 (1C, C_1), 55.0 (2C, OCH_3). ^{11}B NMR (128 MHz, $CDCl_3$) δ: 1.06 ppm. ^{19}F NMR (376 MHz, $CDCl_3$) δ: -139.96 ppm. APCI(+) HRMS calculated for $C_{21}H_{19}BF_2O_4$ [M-F]: 365.1360, found: 365.1365.

(1E,6E)-5-(Difluoroboryloxy)-1,7-bis(2-methoxyphenyl)-1,6-heptadiene-3,5-dione (4). Red solid. Yield: 93% (5.0 g, 13.0 mmol). ^1H NMR (400 MHz, $CDCl_3$) δ (ppm): 8.36 (d, $^3J_{H3\text{-}H4}$ 15.8 Hz, 2H, H_3), 7.60 (dd, $^3J_{H6\text{-}H7}$ 7.8 Hz, *J* 1.8 Hz, 2H, H_6), 7.45 (dt, $J_{H7\text{-}H8\text{-}H9}$ 7.8 Hz, *J* 1.8 Hz, 2H, H_8), 7.03 (dt, $J_{H6\text{-}H7\text{-}H8}$ 7.6 Hz, *J* 1.2 Hz, 2H, H_7), 6.97 (dd, $^3J_{H8\text{-}H9}$ 8.4 Hz, ^4J 1.0 Hz 2H, H_9), 6.90 (d, $^3J_{H3\text{-}H4}$ 15.8 Hz, 2H, H_4), 6.13 (s, 1H, H_1), 3.96 (s, 6H, H_{11}). ^{13}C NMR (150 MHz, $CDCl_3$) δ (ppm): 159.9 ppm (2C, C_2), 142.9 ppm (2C, C_3), 140.5 ppm (2C, C_{10}), 133.9 ppm (2C, C_8), 130.2 ppm (2C, C_6), 124.1 ppm (2C, C_5), 122.0 ppm (2C, C_4), 120.0 ppm (2C, C_7), 111.0 ppm (2C, C_9), 100.4 ppm (1C, C_1), 55,6 ppm (2C, OCH_3). ^{11}B NMR (128 MHz, $CDCl_3$) δ: 1.09 ppm. ^{19}F NMR (376 MHz, $CDCl_3$) δ: -140.67 ppm. APCI(+) HRMS calculated for $C_{21}H_{19}BF_2O_4$ [M-F]: 365.1360, found: 365.1385.

(1E,6E)-5-(Difluoroboryloxy)-1,7-bis-phenyl-1,6-heptadiene-3,5-dione (5). Pink solid. Yield: 85% (3.9 g, 11.9 mmol). ^1H NMR (600 MHz, $CDCl_3$) δ (ppm): 8.10 (d, $^3J_{H3\text{-}H4}$ 15.6 Hz, 2H, H_3), 7.65 (td, $J_{H6\text{-}H7}$ 6.7 Hz, *J* 1.6 Hz, 4H, H_6), 7.49 (m, 6H, $H_{7\text{-}8}$), 6.78 (d, $^3J_{H3\text{-}H4}$ 15,6 Hz, 2H, H_4), 6.15 (s, 1H, H_1). ^{13}C NMR (150 MHz, $CDCl_3$) δ (ppm): 180.3 (2C, C_2), 147.7 (2C, C_4), 134.0 (2C, C_5), 131.9 (4C, C_6), 129.3 (2C, C_8), 129.2 (4C, C_7), 120.6 (2C, C_4), 102.2 (1C, C_1).

^{11}B NMR (128 MHz, $CDCl_3$) δ: 1.06 ppm. ^{19}F NMR (376 MHz, $CDCl_3$) δ: -140.16 ppm. APCI(+) HRMS for $C_{19}H_{15}BF_2O_2$ [M-F] calculated: 305.1149, found: 305.1150.

(1E,6E)-5-(Difluoroboryloxy)-1,7-bis-(4-chlorophenyl)-1,6-heptadiene-3,5-dione (6). Orange solid. Yield: 62% (3.4 g, 8.7 mmol). ^{1}H NMR (400 MHz, $CDCl_3$) δ (ppm): 8.05 (d, $^3J_{H3\text{-}H4}$ 15.6 Hz, 2H, H_3), 7.58 (d, $^3J_{H6\text{-}H7}$ 8.6 Hz, 4H, H_6), 7.45 (d, $^3J_{H6\text{-}H7}$ 8.6 Hz, 4H, H_7), 6.74 (d, $^3J_{H3\text{-}H4}$ 15.6 Hz, 2H, H_4), 6.12 (s, 1H, H_1). ^{13}C NMR (150 MHz, $CDCl_3$) δ (ppm): 180.2 ppm (2C, C_2), 146.2 ppm (2C, C_3), 138.2 ppm (2C, C_8), 132.4 ppm (2C, C_5), 130.3 ppm (4C, C_6), 129.6 ppm (4C, C_7), 120.9 ppm (2C, C_4), 102.5 ppm, (1C, C_1). ^{11}B NMR (128 MHz, $CDCl_3$) δ: 1,01 ppm. ^{19}F NMR (376 MHz, $CDCl_3$) δ: -139,99 ppm. APCI(+) HRMS calculated for $C_{19}H_{13}BCl_2F_2O_2$ [M-F]: 373.0370; found: 373.0370.

(1E,6E)-5-(Difluoroboryloxy)-1,7-bis-(3-chlorophenyl)-1,6-heptadiene-3,5-dione (7). Orange solid. Yield: 69% (3.8 g, 9.7 mmol). ^{1}H NMR (400 MHz, DMSO-*d6*) δ (ppm): 8.05 (d, $^3J_{H3\text{-}H4}$ 12.6 Hz, 2H, H_4), 8.02 (s, 2H, H_{10}), 7.85 (td, $^3J_{H7\text{-}H8}$ 7.6 Hz, *J* 1.5 Hz, 2H, H_8), 7.58 (td, $^3J_{H6\text{-}H7}$ 8.1 Hz, *J* 1.6 Hz, 2H, H_6), 7.53 (t, $J_{H6\text{-}H7\text{-}H8}$ 7.8 Hz, 2H, H_7), 7.39 (d, $^3J_{H3\text{-}H4}$ 15.8 Hz, 2H, H_4), 6.64 (s, 1H, H_1). ^{13}C NMR (150 MHz, DMSO-*d6*) δ (ppm): 180.8 (2C, C_2), 145.8 (2C, C_3), 136.7 (2C, C_9), 134.5 (2C, C_5), 131.9 (2C, C_{10}), 131.5 (2C, C_6), 129.2 (2C, C_8), 128.9 (2C, C_7), 123.5 (2C, C_4), 103.6 (1C, C_1). ^{11}B NMR (128 MHz, DMSO-*d6*) δ: 1.94 ppm. ^{19}F NMR (376 MHz, DMSO-*d6*) δ: -136.93 ppm. APCI(+) HRMS calculated for the ligand (the complex decomposed during sample preparation) $C_{19}H_{14}Cl_2O_2$ [M+H]: 345.0449; found: 345.0428.

(1E,6E)-5-(Difluoroboryloxy)-1,7-bis-(2-chlorophenyl)-1,6-heptadiene-3,5-dione (8). Yellow solid. Yield: 76% (4.2 g, 10.6 mmol). ^{1}H NMR (400 MHz, $CDCl_3$) δ (ppm): 8.48 (d, $^3J_{H3\text{-}H4}$ 15.5 Hz, 2H, H_4), 7.74 (d, $^3J_{H6\text{-}H7}$ 6.9 Hz, 2H, H_6), 7.50 (dd, $^3J_{H8\text{-}H9}$ 7.9 Hz, ^4J 1.4 Hz, 2H, H_9), 7.42 (t, $J_{H7\text{-}H8\text{-}H9}$ 7.6 Hz, 2H, H_8), 7.37 (t, $J_{H6\text{-}H7\text{-}H8}$ 7.4 Hz, 2H, H_7), 6.81 (d, $^3J_{H3\text{-}H4}$ 15.5 Hz, 2H, H_4), 6.24 (s, 1H, H_1). ^{13}C NMR (150 MHz, $CDCl_3$) δ (ppm): 180.7 ppm (2C, C_2), 143.2 ppm (2C, C_3), 136.4 ppm (2C, C_{10}), 132.5 (2C, C_5), 132.2 ppm (2C, C_6), 130.7 ppm (2C, C_9), 128.3 ppm (2C, C_8), 127.3 ppm (2C, C_7), 123,1 ppm (2C, C_4), 102.3 ppm (1C, C_1). ^{11}B NMR (128 MHz, $CDCl_3$) δ: 1,09 ppm. ^{19}F NMR (376 MHz, $CDCl_3$) δ: -139,99 ppm. APCI(+) HRMS calculated for the ligand (the complex decomposed during sample preparation) $C_{19}H_{14}Cl_2O_2$ [M+H]: 345.0449; found: 345.0428.

Photophysical properties

Apparatus: the TDDFT calculations were calculated via Gaussian 16 software[26] on a Linux server. A Perkin Elmer Lambda 35 spectrophotometer was used in UV-Vis measurements, and a Perkin Elmer FL 55 spectrofluorometer for fluorescence measurements respectively. FS5 spectrofluorometer (Edinburgh Instruments) equipped with a 150 W CW ozone free xenon arc lamp, Czerny–Turner monochromators, and a PMT 900 detector was used for determining quantum yields equipped with an integrating sphere featuring a 150 mm PTFE coated internal cavity.

Experimental: for the UV-Vis measurements, a stock solution (100-600 µM) in DMSO was prepared for each compound. From the stock solution consecutive dilutions were made to obtain the UV and fluorescence concentration.

***In silico* experiments:** the first step in the DFT calculation was the optimization of the molecular structures in ground state, followed by the determination of the vertical excitation energies with TDDFT theory for five excited states. Finally, we optimized the molecular structures for five excited states to gain the emission wavelengths. In the case of solutions, PCM model was used. All calculations were carried out using B3LYP function and 6-31+G (d,p) basis sets.

General procedure of the antibacterial experiments

Preparation of microbial strains: each strain (*Escherichia coli* ATCC 25922, *Salmonella enteritidis* ATCC 13076, *Staphylococcus aureus* ATCC 6538P and *Listeria monocytogenes* ATCC 19114) was grown in a test tube

containing 10 mL sterile nutrient broth (Oxoid Ltd., Basingstoke, Hampshire, England) at 37 °C for 24 h. A loopful of inoculum was transferred on selective medium: Baird Parker agar base supplemented with Egg Yolk Tellurite Emulsion for *S. aureus*, TBX agar *for E. coli*, XLD agar for *Salmonella enteritidis* (Oxoid Ltd., Basingstoke, Hampshire, England) and Palcam agar (Oxoid Ltd., Basingstoke, Hampshire, England) for *Listeria monocytogenes.*[27] Plates were incubated for 24 h at 37 °C. Bacterial morphology was confirmed by optical microscopy. After being grown on Mueller Hinton agar (Oxoid Ltd., Basingstoke, Hampshire, UK) for 24 h at 37 °C, several standard culture colonies were transferred into sterile saline solution (8.5 g/L) and adjusted to the turbidity of the McFarland 0.5 standard (1.5×10^6 CFU/mL) [McFARLAND Standards, 28,29].

Agar well diffusion method: the agar plate surface is inoculated by spreading a 100 µL of the microbial inoculum over the entire agar surface. Then, a hole with a diameter of 8 mm is punched aseptically with a sterile punch biopsy, and a volume of 100 µL of the sample is introduced into the well.[30, 31] Then, the plates were incubated at 37 °C for 24 h. The sample diffuses in the agar medium and inhibits the growth of the microbial strain tested. Antibacterial activity was detected by measuring the zone of inhibition (including the wells diameter) appeared after the incubation period. A positive control of gentamicin (0.04 mg/mL in saline solution) was used, while DMSO served as the negative control. For every sample, two replicates were performed.

Acknowledgements

We acknowledge dr. Melinda Gál (National Institute for Research and Development of Isotopic and Molecular Technologies, Cluj-Napoca, Romania) for performing the quantum yield measurements.

Supplementary Material

All data generated or analysed during this research are included in this published article and its supplementary information.

References

1. Anand, P.; Thomas, S. G.; Kunnumakkara, A. B.; Sundaram, C.; Harikumar, K. B.; Sung, B.; Tharakan, S. T.; Misra, K.; Priyadarsini, I. K.; Rajasekharan, K. N.; Aggarwal, B. B. *Biochem. Pharmacol.* **2008**, *76*, 1590–1611. https://doi.org/10.1016/j.bcp.2008.08.008
2. Ayub, H.; Islam, M.; Saeed; M., Ahmad; H., Al-Asmari; F., Ramadan; M. F., Alissa; M., Arif; M. A., Rana; M. U. J., Subtain; M., Rahim; M. A., Zongo; E., Ahmad N. *Food Sci. Nutr.* **2024**, *12*, 8623–8650. https://doi.org/10.1002/fsn3.4469
3. Hu, Y.; Cheng, L.; Du, S.; Wang, K.; Liu, S. *Oncol. Lett.*. **2024**, *27*, 67. https://doi.org/10.3892/ol.2023.14200
4. Alkahtani, S.; S. AL-Johani, N.; Alarifi, S.; Afzal, M. *Int. J. Mol. Sci.* **2023**, *24*, 3842. https://doi.org/10.3390/ijms24043842

5. Larasati, Y. A.; Yoneda-Kato, N.; Nakamae, I.; Yokoyama, T.; Meiyanto, E.; Kato, J. Y. *Sci. Rep.* **2018**, *8*, 2039. https://doi.org/10.1038/s41598-018-20179-6
6. Priyadarsini, K. I. *Molecules*. **2014**, *19*, 20091–20112. https://doi.org/10.3390/molecules191220091
7. Prasad, S.; Dubourdieu, D.; Srivastava, A.; Kumar, P.; Lall, R. *Int. J. Mol. Sci.*. **2021**, *22,* 7094. https://doi.org/10.3390/ijms22137094
8. Tran, Q. H.; Doan, T. T. *New J. Chem.* **2020**, *44*, 13036–13045. https://doi.org/10.1039/D0NJ01159B
9. Hayes, M. R.; Metcalfe, J. *Analyst* **1962**, *87*, 956. https://doi.org/10.1039/AN9628700956
10. Rivoal, M.; Zaborova, E.; Canard, G.; D'Aléo, A.; Fages, F. *New J. Chem.* **2016**, *40*, 1297–1305. https://doi.org/10.1039/C5NJ00925A
11. Gál, E.; Nagy, L. C. *Symmetry.* **2021**, *13*, 2299. https://doi.org/10.3390/sym13122299
12. Pabon, H. J. J. *Recl. Trav. Chim. Pays-Bas.* **1964**, *83*, 379–386. https://doi.org/10.1002/recl.19640830407
13. Rao, E. V.; Sudheer, P. *Indian J. Pharm Sci.* **2011**, *73*, 265-270. https://doi.org/10.4103/0250-474x.93508
14. Gilbert, T.; Morgan, T.; Tunstall, B. *J. Chem. Soc., Trans.* **1924**, *125*, 1963-1967. https://doi.org/10.1039/CT9242501963
15. Crimmins, T. F.; Hauser, C. R. *J. Org. Chem*. **1967**, *32*, 2615-2616. https://doi.org/10.1021/jo01283a055
16. Brown, N. M. D.; Bladon, P. *J. Chem. Soc. A* **1969**, 526-532. https://doi.org/10.1039/J19690000526
17. Felouat, A.; D'Aléo, A. ; Fages, F. *J. Org. Chem.* **2013**, *78*, 4446-4455. https://doi.org/10.1021/jo400389h
18. Canard, G.; Ponce-Vegas, M.; Jaquemin, D.; Le Guenniec, B.; Fellouat, A.; Rivoal, M.; Zabarova, M.; D'Aléo, A.; Fages, F. *RSC Adv.*, **2017**, *7*, 10132. https://doi.org/10.1039/C6RA25436E
19. Liu, K.; Chen, J.; Chojnacki, J.; Zhang, S. *Tetrahedron Lett.*, **2013**, *54*, 2070-2073. https://doi.org/10.1016/j.tetlet.2013.02.015
20. Kabi, A. *J. Chem. Lett.,* **2025**, *6*, 212-222. https://doi.org/10.22034/jchemlett.2025.543299.1340
21. Bellinger, S; Hatamimoshlehabadi, M.; Bag, S.; Mithila, F.; La, J.; Frenette, M.; Laoui, S.; Szlada, D. J.; Yelleswarapu, C. *Chem. Eur. J.* **2018**, *24*, 906–917. https://doi.org/10.1002/chem.201704423
22. Ekici, A. T.; Karakuş, N. *Optik* **2024**, *302*, 171735. https://doi.org/10.1016/j.ijleo.2024.171735
23. Ghosh, R.; Mondal J. A.; Palit, D. K. *J. Phys. Chem. B* **2010**, *114*, 12129–12143. https://doi.org/10.1021/jp1038249
24. Ferreria, J. R. M.; Alves, M.; Sousa, B.; Vieria, S.; Silva, A. M. S.; Guieu, S.; Cunha, A.; Nunes da Silva, R. *Org. Biomol. Chem.*, **2023**, *21*, 1531. https://doi.org/10.1039/D2OB01872A

25. Bakun, P; Kucinska, M.; Kobyłka, P.; Kuźmińska, J.; Koczorowski, T.; Mylnarczyk, D. T.; Popenda, L.; Górska, K.; Kasperkowiak, M.; Murias, M.; Jelińska, A.; Goslinski, T. *Med. Chem. Res.* **2024**, *33*, 944-963.
26. Gaussian 16, Revision C.01, Frisch, M. J.; Trucks, G. W.; Schlegel, H. B.; Scuseria, G. E.; Robb, M. A.; Cheeseman, J. R.; Scalmani, G.; Barone, V.; Petersson, G. A.; Nakatsuji, H.; Li, X.; Caricato, M.; Marenich, A. V.; Bloino, J.; Janesko, B. G.; Gomperts, R.; Mennucci, B.; Hratchian, H. P.; Ortiz, J. V.; Izmaylov, A. F.; Sonnenberg, J. L.; Williams-Young, D.; Ding, F.; Lipparini, F.; Egidi, F.; Goings, J.; Peng, B.; Petrone, A.; Henderson, T.; Ranasinghe, D.; Zakrzewski, V. G.; Gao, J.; Rega, N.; Zheng, G.; Liang, W.; Hada, M.; Ehara, M.; Toyota, K.; Fukuda, R.; Hasegawa, J.; Ishida, M.; Nakajima, T.; Honda, Y.; Kitao, O.; Nakai, H.; Vreven, T.; Throssell, K.; Montgomery, J. A., Jr.; Peralta, J. E.; Ogliaro, F.; Bearpark, M. J.; Heyd, J. J.; Brothers, E. N.; Kudin, K. N.; Staroverov, V. N.; Keith, T. A.; Kobayashi, R.; Normand, J.; Raghavachari, K.; Rendell, A. P.; Burant, J. C.; Iyengar, S. S.; Tomasi, J.; Cossi, M.; Millam, J. M.; Klene, M.; Adamo, C.; Cammi, R.; Ochterski, J. W.; Martin, R. L.; Morokuma, K.; Farkas, O.; Foresman, J. B.; Fox, D. J. Gaussian, Inc., Wallingford CT, 2016.
27. Bodea, I. M.; Cătunescu, G. M.; Pop, C. R.; Fiț, N. I.; David, A. P.; Dudescu, M. C.; Stănilă, A.; Rotar, A. M.; Beteg, F. I. *Polymers* **2022**, *14*, 1435. https://doi.org/10.3390/polym14071435
28. Semeniuc, C. A.; Pop, C. R.; Rotar, A. M. *J. Food Drug Anal.* **2017**, *25*, 403–408. https://doi.org/10.1016/j.jfda.2016.06.002
29. Cerezo, A. B.; Cătunescu, G. M.; González, M. M.-P.; Hornedo-Ortega, R.; Pop, C. R.; Rusu, C. C.; Chirilă, F.; Rotar, A. M.; Garcia-Parrilla, M. C.; Troncoso, A. M. *Antioxidants* **2020**, *9*, 478. https://doi.org/10.3390/antiox9060478
30. Gonelimali, F. D.; Lin, J; Miao, W; Xuan, J.; Charles, F; Chen, M; Hatab, S. R. *Front. Microbiol.* **2018**, *9*, 1639. https://doi.org/10.3389/fmicb.2018.01639
31. Balouiri, M.; Sadiki, M.; Ibnsouda, S. K. *J. Pharm. Anal.* **2016**, *6*, 71–79. https://doi.org/10.1016/j.jpha.2015.11.005